Science of the Total Environment 903 (2023) 166162

Contents lists available at ScienceDirect

Science of the Total Environment

journal homepage: www.elsevier.com/locate/scitotenv

Modeling of secondary organic aerosols (SOA) based on two commonly used air quality models in China: Consistent S/IVOCs contribution but large differences in SOA aging

Ling Huang [a], Hanqing Liu [a], Greg Yarwood [b,*], Gary Wilson [b], Jun Tao [c], Zhiwei Han [d], Dongsheng Ji [e], Yangjun Wang [a], Li Li [a,*]

[a] School of Environmental and Chemical Engineering, Shanghai University, Shanghai 200444, China
[b] Ramboll, Novato, California 94945, USA
[c] Institute for Environmental and Climate Research, Jinan University, Guangzhou 510632, China
[d] University of Chinese Academy of Sciences, Beijing 100049, China
[e] Institute of Atmospheric Physics, Chinese Academy of Sciences, Beijing 100029, China

HIGHLIGHTS

- Simulated SOA contributions from different precursors using two commonly used models, CAMx and CMAQ, were contrasted.
- IVOC represents an important SOA precursor while SOA contributions from SVOC emissions are negligible.
- Different treatments of SOA aging are responsible for different ASOA produced from anthropogenic VOCs.

GRAPHICAL ABSTRACT

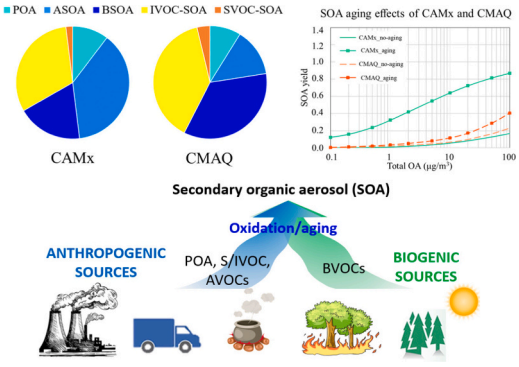

ARTICLE INFO

Editor: Jianmin Chen

Keywords:
Secondary organic aerosols
Air quality modeling
SOA aging

ABSTRACT

Secondary organic aerosol (SOA) is an important component of atmospheric fine particulate matter ($PM_{2.5}$), with contributions from anthropogenic and biogenic volatile organic compounds (AVOC and BVOC) and semi- (SVOC) and intermediate volatility organic compounds (IVOC). Policymakers need to know which SOA precursors are important but accurate simulation of SOA magnitude and contributions remain uncertain. Findings from existing SOA modeling studies have many inconsistencies due to differing emission inventory methodologies/assumptions, air quality model (AQM) algorithms, and other aspects of study methodologies. To address some of the inconsistencies, we investigated the role of different AQM SOA algorithms by applying two commonly used models, CAMx and CMAQ, with consistent emission inventories to simulate SOA concentrations and contributions for July and November 2018 in China. Both models have a volatility basis set (VBS) SOA algorithm but with different parameters and treatments of SOA photochemical aging. SOA generated from BVOC (i.e., BSOA) is found to be more important in southern China. In contrast, SOA generated from anthropogenic precursors is

* Corresponding authors.
E-mail addresses: gyarwood@ramboll.com (G. Yarwood), lily@shu.edu.cn (L. Li).

https://doi.org/10.1016/j.scitotenv.2023.166162
Received 9 May 2023; Received in revised form 3 August 2023; Accepted 7 August 2023
Available online 11 August 2023

more prevalent in the North China Plain (NCP), Yangtze River Delta (YRD), Sichuan Basin and Central China. Both models indicate negligible SOA formation from SVOC emissions compared to other precursors. In July, when BVOC emissions are abundant, SOA is predominantly contributed by BSOA (except for NCP), followed by IVOC-SOA (i.e., SOA produced from IVOC) and ASOA (i.e., SOA produced from anthropogenic VOC). In contrast, in November, IVOC became the leading SOA contributor for all selected regions except PRD, illustrating the important contribution of IVOC emissions to SOA formation.

While both models generally agree in terms of the spatial distributions and seasonal variations of different SOA components, CMAQ tends to predict higher BSOA, while CAMx generates higher ASOA concentrations. As a result, CMAQ results suggest that BSOA concentration is always higher than ASOA in November, while CAMx emphasizes the importance of ASOA. Utilizing a conceptual model, we found that different treatment of SOA aging between the two models is a major cause of differences in simulated ASOA concentrations. The step-wise SOA aging scheme implemented in the CAMx VBS (based on gas-phase reactions with OH radical and similar to other models) exhibits a strong enhancement effect on simulated ASOA concentrations, and this effect increases with the ambient organic aerosol (OA) concentrations. The CMAQ aerosol module implements a different SOA aging scheme that represents particle-phase oligomerization and has smaller impacts on total OA. Different structures and/or parameters of the SOA aging schemes are being used in current models, which could greatly affect model simulations of OA in ways that are difficult to anticipate. Our results indicate that future control policies should aim at reducing IVOC emissions as well as traditional VOC emissions. In addition, aging schemes are the major driver in CMAQ vs. CAMx treatments of ASOA and their resulting predicted mass. More sophisticated measurement data (e.g., with resolved OA components) and/or chamber experiments (e.g., investigating how aging influences SOA yields) are needed to better characterize SOA aging and constrain model parameterizations.

1. Introduction

Atmospheric fine particulate matter ($PM_{2.5}$) could reduce visibility (Kampa and Castanas, 2008), affect regional climate directly or indirectly (Liu et al., 2014), and exhibit adverse impacts on public health (Xie et al., 2014; Zhang et al., 2007). With the substantial emission reduction of sulfur dioxide (SO_2), nitrogen oxides (NO_x), and primary particles in China over the past decade (Yan et al., 2021; Zheng et al., 2018), the organic portion of $PM_{2.5}$ has become increasingly important. Observations show that organic aerosols (OA) could contribute 30–70 % of total $PM_{2.5}$ in China, with the secondary portion (i.e., secondary organic aerosols, SOA) accounting for a more significant portion than the primary portion (i.e., primary organic aerosols, POA) (Li et al., 2016a; Shi et al., 2016). SOA is formed via chemical reactions of anthropogenic and biogenic precursors (e.g., volatile organic compounds, VOC) followed by subsequent gas-particle partitioning processes (Murphy et al., 2006). A recent study by (Pye et al., 2021) reported that SOA is associated with a higher rate of cardiorespiratory mortality than $PM_{2.5}$ on a per-mass basis.

Numerical air quality models (AQM) are essential tools to evaluate the effectiveness of emission control policies, quantify regional contributions, and predict concentrations under future emission scenarios. However, accurate simulation of the magnitudes and variations of SOA via AQM has always been challenging due to the complexity of SOA itself and the complicated chemical processes involved in SOA formation. Table S1 summarizes existing SOA simulation studies by different AQMs in China during the past ten years, including the Community Multiscale Air Quality (CMAQ) modeling system, Weather Research and Forecasting model coupled with Chemistry (WRF-Chem), the Comprehensive Air-quality Model with Extensions (CAMx), the Goddard Earth Observing System-Chem (GEOS-Chem), and other models. The SOA formation modules within these AQMs models generally apply either the two-product approach (Odum et al., 1996) and/or the volatility basis set (VBS) approach (Donahue et al., 2006), with the former easy to implement and the latter better at capturing the SOA chemical aging (An et al., 2022; Lin et al., 2016; Yao et al., 2020). Earlier modeling studies utilizing the two-product approach usually underestimated SOA. For example, Jiang et al. (2012) found a maximum underestimation of 75 % in simulated SOA during 2016 over China. In another study by Li et al. (2017b), although simulated SOA concentration increased nearly four times after increasing aromatic emissions and changing SOA yields, the model still underestimated observed SOA by 72 % on average. To better represent the physical and chemical attributes of SOA in AQMs, Donahue et al. (2006) introduced the VBS scheme, which considers gas-aerosol partitioning and chemical aging of both POA and SOA. Compared to the two-product approach, VBS is shown to improve model simulations of SOA substantially. Han et al. (2016) simulated SOA in eastern China and found that the VBS approach could well reproduce the observed SOA at four monitoring sites both in magnitudes (2.8 $\mu gC/m^3$ vs. observed value of 3.3 $\mu gC/m^3$) and in terms of the SOA/OA ratio (33 % vs. observed value of 32 %). Lin et al. (2016) applied the VBS approach in CAMx to simulate SOA concentration and source attribution in Beijing urban area in the summer; results show that the VBS approach substantially improved simulated SOA concentration (from 0.73 $\mu g/m^3$ to 5.3 $\mu g/m^3$ at a station in Beijing); however, the model still underpredicted observed SOA values with NMB of −72 %. Due to the significant computational cost, current AQMs cannot adopt explicit chemical mechanisms for SOA parameterizing. This limitation consequently leads to a degradation of its model performance. Recent studies show promising results in predicting SOA and quantifying its sources based on machine learning techniques (e.g., Pande et al., 2022; Qin et al., 2022; Schreck et al., 2022). For instance, Wang et al. (2022) resolved the importance of different VOCs on SOA in Tianjin based on the random forest (RF) model. Wang et al., 2022 successfully applied the RF algorithm to predict the concentrations of POA and oxygenated organic aerosols at different sites in Hong Kong. Schreck et al. (2022) demonstrated the ability of neural network models to accurately emulate SOA formation from an explicit model with small error.

In addition to SOA module improvements, the inclusion of semi-volatile and intermediate-volatility organic compounds (S/IVOC) emissions has also been shown to reduce the gap between observed and simulated SOA concentrations, although uncertainties exist with the estimated S/IVOC emissions (Table S2). For example, the inclusion of IVOC emissions was shown to increase the simulated SOA concentration by 5 %–26 % at an observation site in the Yangtze River Delta (YRD) region (Huang et al., 2021a). With an updated national S/IVOC emission inventory, the average deviation between simulated and observed SOA concentrations in China was reduced by 25 % (Wu et al., 2021b). Regional or national emission inventory of S/IVOC emissions were estimated based on either the conventional emission ratio method (i.e., ratio based on POA, VOC, or naphthalene, Wu et al., 2021b) or using directly measured emission factor (Liu et al., 2017; Wu et al., 2021b). Chang et al. (2022) proposed a full-volatility organic emission inventory recognizing that emissions of organic compounds have a continuous spectrum spanning from low to high volatility.

Although substantial progress has been made in improving SOA

simulation, inconsistent findings were reported among recent SOA modeling studies in China, which warrants further investigation. For example, Miao et al. (2021) simulated much higher wintertime SOA concentrations over eastern China than summertime SOA. In contrast, An et al., 2022 and Chang et al. (2022) reported slightly higher SOA in summer. Both Chang et al. (2022) and Wu et al. (2021b) reported higher SOA formed from IVOC emissions (IVOC-SOA) than SVOC (SVOC-SOA), which is opposite to Miao et al.'s (2021) results showing much higher (by as much as two times) SVOC-SOA than IVOC-SOA in eastern China. The simulated SOA from conventional anthropogenic VOC (ASOA) also differs among studies. ASOA is estimated to be negligible (~0.25 μg m^{-3}) over the YRD region, and adding I/SVOC emissions increased SOA concentration by 116 % (An et al. (2022). On the contrary, anthropogenic VOC (AVOC) are reported to contribute most to SOA formation (35.6–59.1 %) and S/IVOC contributed the least (6.0–10.6 %) in Li et al. (2022). These inconsistencies are potentially due to different S/IVOC emission inventories and different SOA modules being applied, which limits a direct comparison.

CAMx and CMAQ are two frequently used models to address various air pollution questions, partially due to their ability to track source contribution (Cao et al., 2022; Li et al., 2016b; Zhang et al., 2018). Both models incorporated the VBS scheme to simulate SOA, but their simulation results have not been compared with each other. Therefore, this study attempts to resolve some of the existing inconsistencies of simulated SOA by a detailed comparison between two commonly used air quality models – CAMx and CMAQ. A publicly available national S/IVOC emission inventory developed for China was used in both models to facilitate direct comparison while temporarily ignoring the uncertainties associated with the S/IVOC emission inventory itself. Similarities and differences in the simulated results from the two models are considered with a focus on contributions of different emission types (POA, VOC, IVOC, SVOC) and the SOA aging schemes which differ. Results from this study illustrate the uncertainties associated with SOA schemes in AQMs even when the model input data are harmonized. Revealing the important influence of SOA aging can stimulate future improvements to SOA modeling schemes.

2. Methodology

2.1. Model configuration

In this study, two commonly used air quality models - CAMx version 7.10 (Ramboll, 2021) and CMAQ version 5.3.2 (US EPA, 2020) were used to simulate SOA concentrations in China for July (representing summer) and November (representing fall) of the calendar year 2018. The models are applied over the same domain with input data developed from the same sources, although each model has its own processes for handling input data. Table 1 summarizes the key differences in model configurations between the two models. The modeling domain covers China with a spatial resolution of 36 km (Fig. 1). The Weather Research and Forecasting (WRF) model (version 4.0, Skamarock and Klemp, 2008) was applied to simulate meteorological fields, and WRF model configurations were summarized in our previous studies (Huang et al., 2023; Huang et al., 2021b). Anthropogenic emissions within China utilized the Multi-resolution Emission Inventory for 2017 (MEIC, Zhang et al., 2019) developed by Tsinghua University; emissions outside China are based on the Emissions Database for Global Atmospheric Research (EDGAR, Li et al., 2017a) for the year 2010.

The CAMx model configuration included the CB6 photochemical gas-phase mechanism (Yarwood et al., 2010), the static two-mode coarse/fine (CF) PM chemistry option with ISORROPIA inorganic gas-aerosol partitioning scheme (Nenes et al., 1998), the Regional Acid Deposition Model (RADM) aqueous phase chemistry, the Zhang dry deposition option (Zhang et al., 2003) and wet deposition. In terms of the SOA modeling scheme, CAMx provides the option to select one of two schemes: a traditional two-product scheme (named SOAP) or a 1.5-D VBS scheme which is a simplified version of the 2-D VBS scheme (Koo et al., 2014). This study used the CAMx 1.5D VBS scheme because it is more similar to the VBS in the CMAQ SOA aerosol module. Compared with the SOAP scheme, the 1.5-D VBS scheme treats POA as being semivolatile and includes multi-stage aging of SOA with both oxidation and fragmentation occurring to describe the evolution of OA in terms of oxidation state and volatility. For CMAQ simulations, the model configuration included the CB6 gas-phase mechanism, the RADM aqueous phase chemistry, ISORROPIA inorganic particulate thermodynamics, and the AERO7 aerosol scheme (Appel et al., 2021).

Both CMAQ and CAMx consider SOA formation from traditional anthropogenic VOC (e.g., benzene, toluene, and xylene) and biogenic VOC (i.e., isoprene, monoterpenes and sesquiterpenes emitted by vegetation), but there are several differences. For instance, CMAQ includes SOA formation from isoprene oxidation product (ioprene epoxydiol, IEPOX) in the aqueous phase (Pye et al., 2017; Pye et al., 2013), organic nitrate from monoterpene oxidation (Pye et al., 2015), SOA formed from glyoxal and methylglyoxal uptake to particles (Pye et al., 2015) and in clouds (Carlton et al., 2008). Important differences exist in the VBS framework between the CAMx 1.5D VBS and CMAQ AERO7 schemes. In CAMx, SOA formation from all precursors is treated in a VBS style, and each volatility bin can be oxidized continuously to the next lower volatility bin in a step-wise manner providing a dynamic SOA volatility distribution. Aging of BSOA is disabled due to over-prediction

Table 1
Summary of model differences between CAMx and CMAQ.

Model	CAMx	CMAQ
version	7.10	5.3.2
Gas-phase mechanism	CB6	CB6
SOA module	1.5D VBS: step-wise aging of anthropogenic SOA; no aging for BSOA and biomass burning SOA	AERO7: VBS style for anthropogenic SOA; aging is partially represented by oligomers;
Aqueous formation of BSOA	Formation from alpha-dicarbonyls	Formation from IEPOX and alpha-dicarbonyls
IVOC emissions	Renamed as IVOA/IVOB/IVOG/IVOD	mapped to pcVOC
SVOC emissions	Renamed as POA_GV/POA_DV/POA_OP/POA_BB	Allocated to CMAQ species based on default ratio

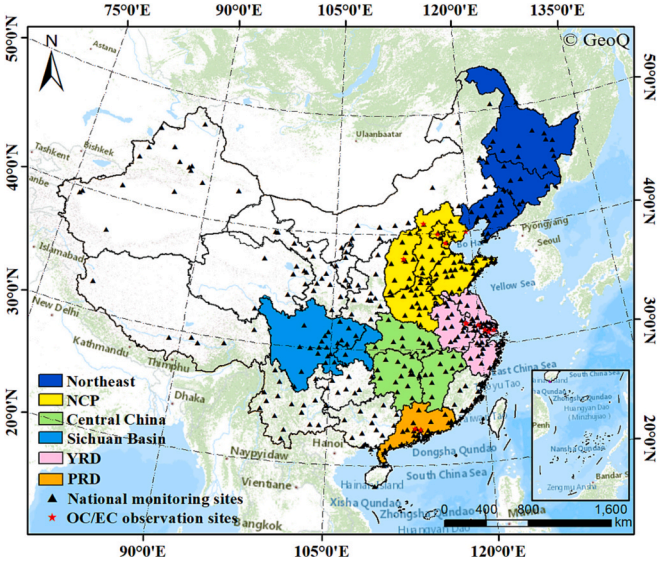

Fig. 1. Modeling domain with definitions of key regions and locations of national monitoring sites (in black triangles) in major cities and sites with OC/EC observations (in red star) in 13 cities.

of OA in rural areas reported in previous studies (Koo et al., 2014). On the other hand, CMAQ treats some SOA formation pathways (e.g., oxidation of VOC and SVOC) in a VBS style and others not (e.g., aqueous pathways and pcVOC oxidation). The SOA formed with VBS treatment in CMAQ does not undergo further oxidation, so a static volatility distribution is maintained. Oligomerization of the condensed aerosol was considered to partially account for SOA aging in CMAQ (Carlton et al., 2010; Pye and Pouliot, 2012). This point will be discussed further in Section 3.4.

2.2. VOC/SVOC/IVOC emissions

Conventional anthropogenic VOC emissions were provided in the MEIC inventory, while biogenic VOC emissions were calculated using a recent offline version of the Model of Emissions of Gases and Aerosols from Nature (version 3.2, https://bai.ess.uci.edu/megan). Specifically, MEIC provides VOC emissions speciated for Carbon Bond 2005 (CB05) and SAPRC 2007 (SAPRC07), which were combined to generate speciated VOC emissions for the CB6 mechanism (see Supplemental text 1). To evaluate the contributions of SVOC and IVOC emissions to SOA formation, we included a gridded (0.25° × 0.25°) monthly S/IVOC emission inventory from industry, residential, transportation, power plants, and shipping for the year 2016, which was developed by applying source-specific emission ratio of S/IVOC to POA (Wu et al., 2021a). The total reported SVOC and IVOC emissions were 2881 and 6718 Gg, respectively, with industry and residential sectors being the dominant contributor. On an annual scale, industrial and residential sources accounted for 12.6 % and 64.6 % of the total SVOC emissions and 63.1 % and 15.5 % of the total IVOC emissions. Spatially, S/IVOC emissions are mainly distributed in China's highly industrialized and urbanized regions, for example, the Beijing-Tianjin-Hebei (BTH) and YRD regions (Wu et al., 2021b). Regarding the monthly variations, S/IVOC emissions are higher in winter (due to residential sources) and lower in summer, with winter season (i.e., three months) emissions accounting for 31 % of annual total emissions.

For the CAMx simulations, IVOC were labelled as 'IVOG', 'IVOD', 'IVOB', and 'IVOA', each representing IVOC emissions from gasoline engines, diesel engines, biomass burning, and other anthropogenic sources; the corresponding SVOC was renamed as 'POA_GV', 'POA_DV', 'POA_BB' and 'POA_OP' (Ramboll, 2021). In CMAQ simulations, IVOC were directly mapped to pcVOC, the precursor of potential SOA formation from combustion emissions (pcSOA). According to (Murphy et al., 2017), pcSOA was introduced to compensate for missing SOA mass from sources such as IVOC oxidation, aging of secondary organic vapors, biases in SOA yields due to vapor wall losses, enhanced organic partitioning, and oxidation of unidentified SOA precursors. In the default CMAQ v5.3.2, pcVOC is scaled to the POA emissions using a constant scaling factor. A detailed comparison of the emission magnitudes as well as the corresponding SOA yields of the IVOC emissions used in this study and the pcVOC emissions calculated based on the CMAQ default scaling factor was provided in Supplemental text 2. SVOC were allocated into CMAQ semivolatile species based on existing ratios provided (Donahue et al., 2006; Murphy et al., 2017; see Table S6 for details).

2.3. Simulation scenarios

In order to evaluate the impact of different models and VOC/SVOC/IVOC emissions on simulated SOA concentration, three sets of parallel simulations (each set with CMAQ and CAMx, respectively, so a total of six) were conducted for July and November 2018 with identical meteorological fields (Table 2). In the base scenarios ('CAMx_base' and 'CMAQ_base'), only the conventional anthropogenic emissions and biogenic emissions were included. The simulated SOA in these base scenarios is the sum of ASOA and BSOA. In the second set of IVOC scenarios ('CAMx_IVOC' and 'CMAQ_IVOC'), IVOC emissions were included, and the simulated SOA now includes ASOA, BSOA, and IVOC-SOA. In the final set of S/IVOC scenarios ('CAMx_S/IVOC' and 'CMAQ_S/IVOC'), both IVOC and SVOC emissions were included. The contribution of IVOC and SVOC emissions to SOA was quantified by subtracting the base case results from the corresponding scenarios (e.g., 'CAMx_IVOC' minus 'CAMx_base' to get IVOC contribution, etc.). Different OA components, including POA, anthropogenic SOA (ASOA), and biogenic SOA (BSOA), were distinguished in each scenario because they are resolved by the model OA schemes.

Table 2
Model scenarios.

Scenario	AQM	Anthropogenic VOC emissions	IVOC emissions	SVOC emissions
CAMx_base	CAMx v7.10	MEIC	None	None
CAMx_IVOC		MEIC	Wu et al. (2021a, 2021b)	None
CAMx_S/IVOC		MEIC	Wu et al. (2021a, 2021b)	Wu et al. (2021a, 2021b)
CMAQ_base	CMAQ v5.3.2	MEIC	None	None
CMAQ_IVOC		MEIC	Wu et al. (2021a, 2021b)	None
CMAQ_S/IVOC		MEIC	Wu et al. (2021a, 2021b)	Wu et al. (2021a, 2021b)

2.4. $PM_{2.5}$ and OC/EC observations

Simulated concentrations of $PM_{2.5}$ and secondary organic carbon (SOC) were compared against surface observations of hourly $PM_{2.5}$ at 364 national monitoring sites, and organic carbon (OC)/elemental carbon (EC) were compared at a limited number of sites. Observations of $PM_{2.5}$ were obtained from the China National Environmental Monitoring Centre (http://www.cnemc.cn/, accessed on 25th September 2021). Hourly observed OC/EC during July and November 2018 at 13 monitoring sites (see detailed locations in Table S7) were used to evaluate simulated SOA by applying the minimum OC/EC ratio method (Cao et al., 2004; Castro et al., 1999) to the observations. The OC/EC sites were mainly located in North China, East China, and South China. Model performance was evaluated based on commonly used statistical metrics, including the mean bias (MB), normalized mean bias (NMB), normalized mean error (NME), and FAC2 (see Table S8 for definitions).

3. Results and discussions

3.1. Model performance evaluation

Fig. 2 shows the spatial distribution of monthly averaged $PM_{2.5}$ concentration simulated under CAMx_S/IVOC and CMAQ_S/IVOC scenarios. Overall, the two models are able to capture the spatial distributions and seasonal variations of observed $PM_{2.5}$ with MB of −4.1–8.3 μg m^{-3}, NMB of −17.1–17.5 %, and NME of 37–49 %. Values of NMB and NME meet the criteria standards (NMB within 20 % and NME within 45 %, except for CAMx NME) proposed by (Huang et al., 2021c), indicating acceptable model performance for $PM_{2.5}$. Regionally, simulations over NCP and Sichuan Basin show an overestimation with MB of −8.2–24.8 μg m^{-3} and NMB of −16.0–59.6 % (Table S9). CAMx generally tends to simulate higher $PM_{2.5}$ concentrations (by 13.4–60.2 %) than CMAQ. We further evaluated simulated SOC at a limited number of observation sites (Fig. S2 and Fig. S3), noting that the "measured" SOC is diagnosed from measurements of total OC as discussed above. Model performance for simulated SOC varies across different sites, with a general pattern of overestimation in July and underestimation in November (Table S10).

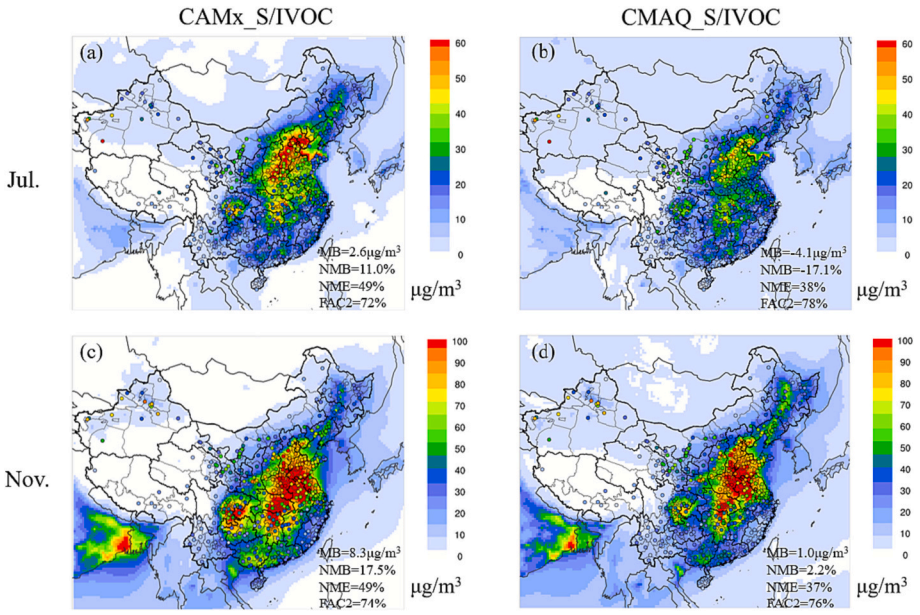

Fig. 2. Spatial distributions of simulated and observed (filled circles) $PM_{2.5}$ concentration (μg/m) in July (upper row) and November (bottom row) 2018 based on CAMx (left column) and CMAQ (right column) simulations, including S/IVOC emissions.

3.2. OA components simulated by CAMx and CMAQ

Fig. 3 shows the spatial distribution of different OA components simulated by CAMx and CMAQ for July and November. Five OA components, including POA, ASOA, IVOC-SOA, SVOC-SOA, and BSOA, were identified as direct model outputs (i.e., POA and BSOA) or obtained as the differences between different modeling scenarios listed in Table 2. Figs. 4 and 5 show the subdomain averaged relative contribution of different OA components for selected regions for July and November, respectively. The spatial distributions of relative percentages of each SOA component are shown in Fig. S4. Table S11 shows the domain averaged concentration for each OA component by selected regions.

3.2.1. Primary organic aerosols (POA)

POA represents organic aerosols that are directly emitted from anthropogenic sources (e.g., residential wood combustion). In the VBS scheme, POA is allowed to vaporize into the gaseous phase and undergo further oxidation processes to form SOA. The magnitudes and spatial distributions of POA agree well between CAMx and CMAQ results as well as previous studies (e.g., Hu et al., 2017), with high concentrations simulated over Northeast China, NCP, northern YRD, and Sichuan Basin. Seasonally, simulated POA concentration in November is much higher than in July due to higher emissions. In July, POA ranged from 0.3 μg/m^3 in PRD (simulated by CMAQ) to 1.9 μg/m^3 in Sichuan Basin (simulated by CAMx) and accounts for <10 % of the total OA concentrations for all selected regions, except Sichuan Basin (~15 %), suggesting a

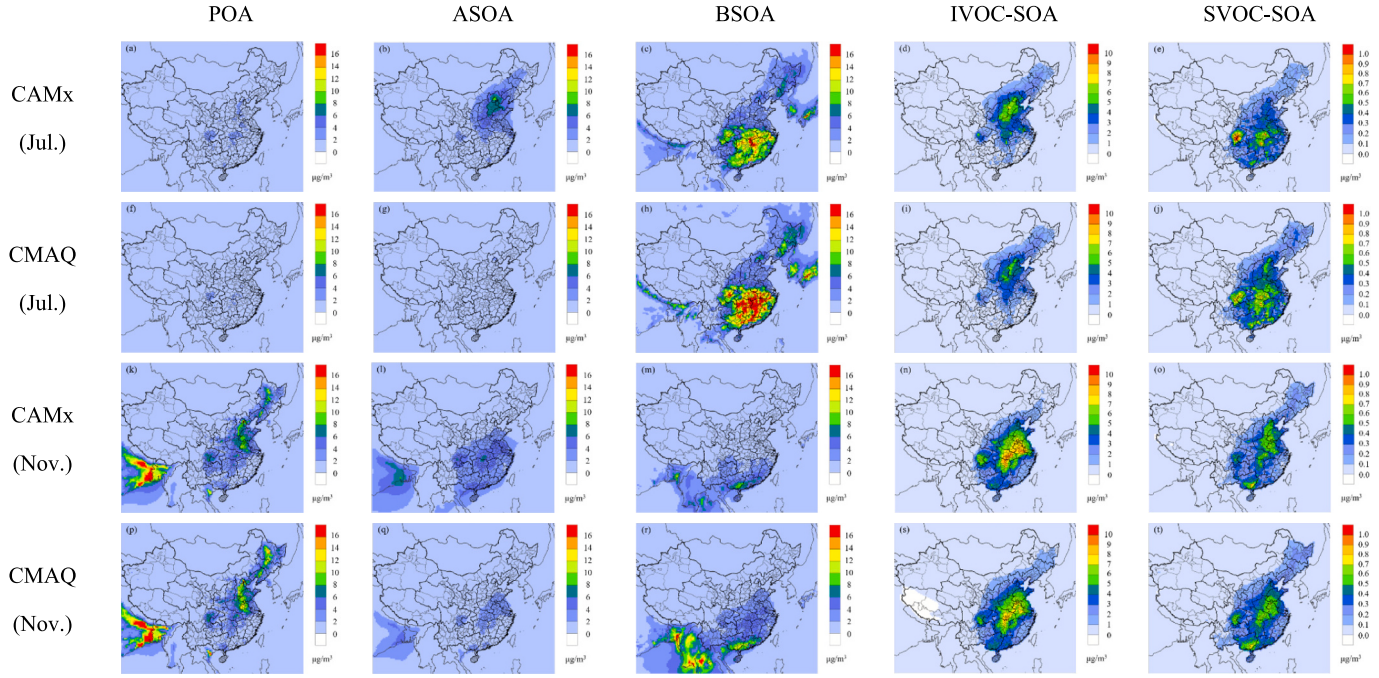

Fig. 3. Spatial distributions of different OA components in July and November.

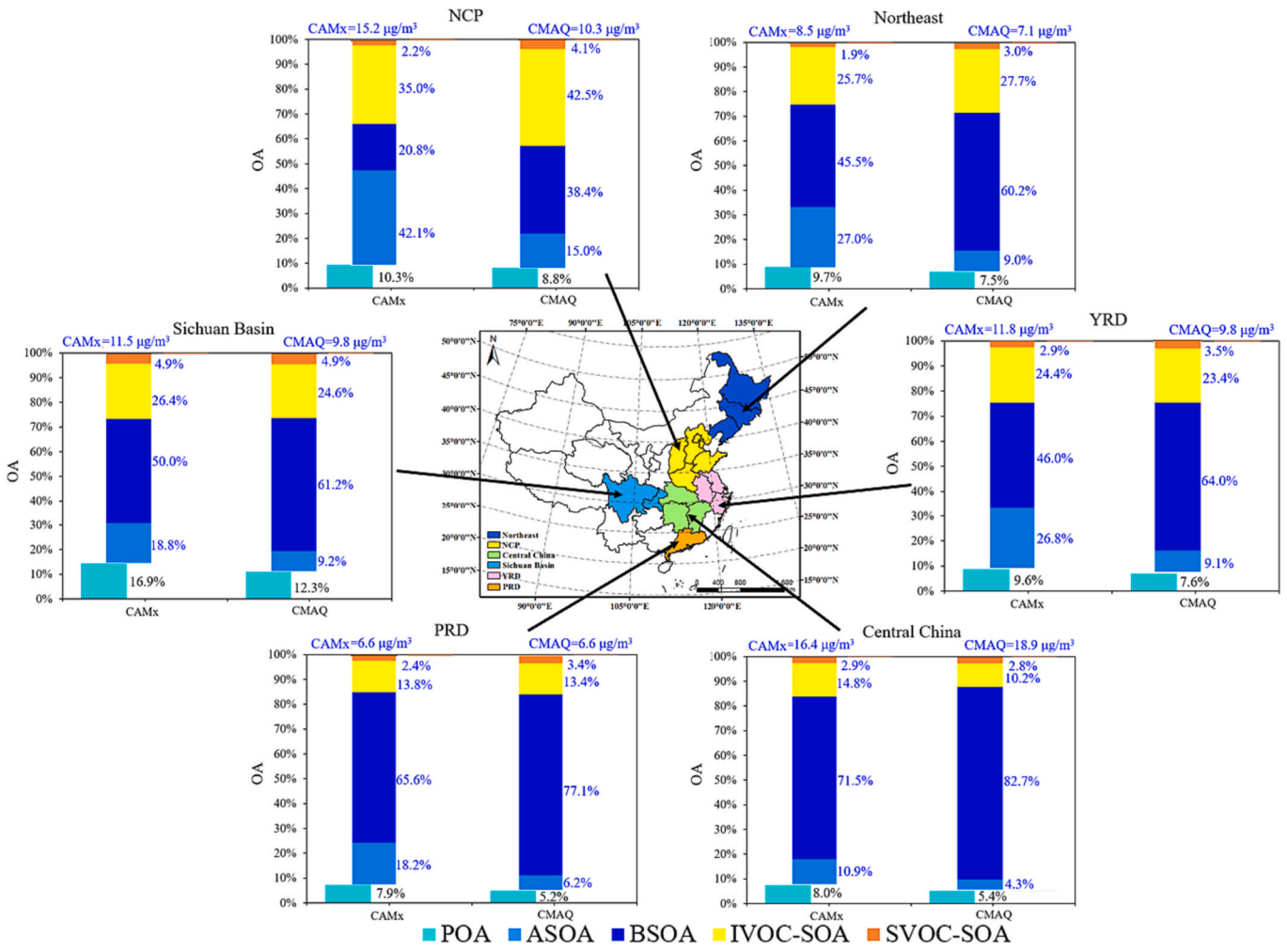

Fig. 4. Domain-averaged OA concentration (labelled on top) and relative contributions of different components (labelled inside Figures) in July 2018 (Note that the relative contributions of ASOA, BSOA, IVOC-SOA, and SVOC-SOA sum to 100 %).

relatively minor role compared to SOA during the summer season. In November, domain-averaged POA ranged from 1.3 μg/m^3 in PRD (simulated by CMAQ) to 6.7 μg/m^3 in Northeast (simulated by CMAQ) and became the dominant OA component in Northeast China (~70 %). For other regions in November, POA contributed from ~10 % (in PRD) to ~40 % (in NCP) of the total OA concentration, suggesting that SOA is still the dominant OA component for most regions.

3.2.2. *Secondary organic aerosols (SOA)*

Except for Northeast China in November, SOA concentration exceeds that of POA, and different SOA components show distinctly different seasonal and spatial variations. Biogenic SOA (BSOA) is mainly concentrated in southern China, where BVOC emissions are abundant (Fig. S5). In contrast, anthropogenic-oriented SOA (i.e., ASOA and IVOC-SOA) are mainly concentrated over northern China in July and shifted southward in November. Seasonally, BSOA concentration is much higher in July, with maximum monthly-averaged BSOA concentration exceeding 15 μg/m^3 over specific areas in Central China. In contrast, most regions had higher ASOA and IVOC-SOA concentrations in November. Figs. 4 and 5 show the subdomain averaged relative contribution of different OA components for selected regions. In July, BSOA represented the dominant SOA component (except NCP), accounting for 45.5 % – 60.2 % in the Northeast to as much as 71.5 % – 82.7 % in Central China. In November, when BVOC emissions are dramatically lower, the relative contribution of BSOA decreases sharply. Nevertheless, BSOA still represents the most abundant SOA component (37.1 % – 51.0 %) for PRD in November.

Differences are observed in the magnitude of simulated BSOA and ASOA concentrations between the two models, although the spatial distributions and seasonal variations are consistent. On the one hand, CMAQ tends to simulate slightly higher BSOA concentrations than CAMx. For example, the domain averaged BSOA concentration over NCP in July is 2.8 μg/m^3 based on CAMx results, which is 22.2 % lower than that of CMAQ. For Central China, where BVOC emissions are abundant, BSOA estimated from CAMx in July (10.8 μg/m^3) is 33.1 % lower than CMAQ (14.8 μg/m^3). In November, the relative differences in BSOA between the two models become even larger, although the absolute magnitudes are lower compared to July. The higher BSOA simulated by CMAQ is likely associated: (1) the yield of organic aerosol from monoterpene oxidation was increased (Xu et al., 2018); (2) alpha-pinene was treated explicitly in the model, and 30 % of the total terpenes emissions were allocated to alpha-pinene (Pye et al., 2010) and (3) more BSOA formation pathways are included in CMAQ, for example, the aqueous SOA formation from IEPOX (Pye et al., 2017; Pye et al., 2013). However, we did not investigate this difference because our study focuses on anthropogenic emissions. On the other hand, CAMx predicts much higher ASOA concentration than CMAQ, by up to ~ four times higher in July and ~ 2 times higher in November. For instance, CAMx simulated ASOA concentration in NCP is 5.7 μg/m^3 for July instead of 1.4 μg/m^3 by CMAQ. CAMx simulated ASOA concentration in YRD in November was 4.1 μg/m^3 compared to 2.4 μg/m^3 by CMAQ. This difference in simulated ASOA concentration is discussed in detail in Section 3.4.

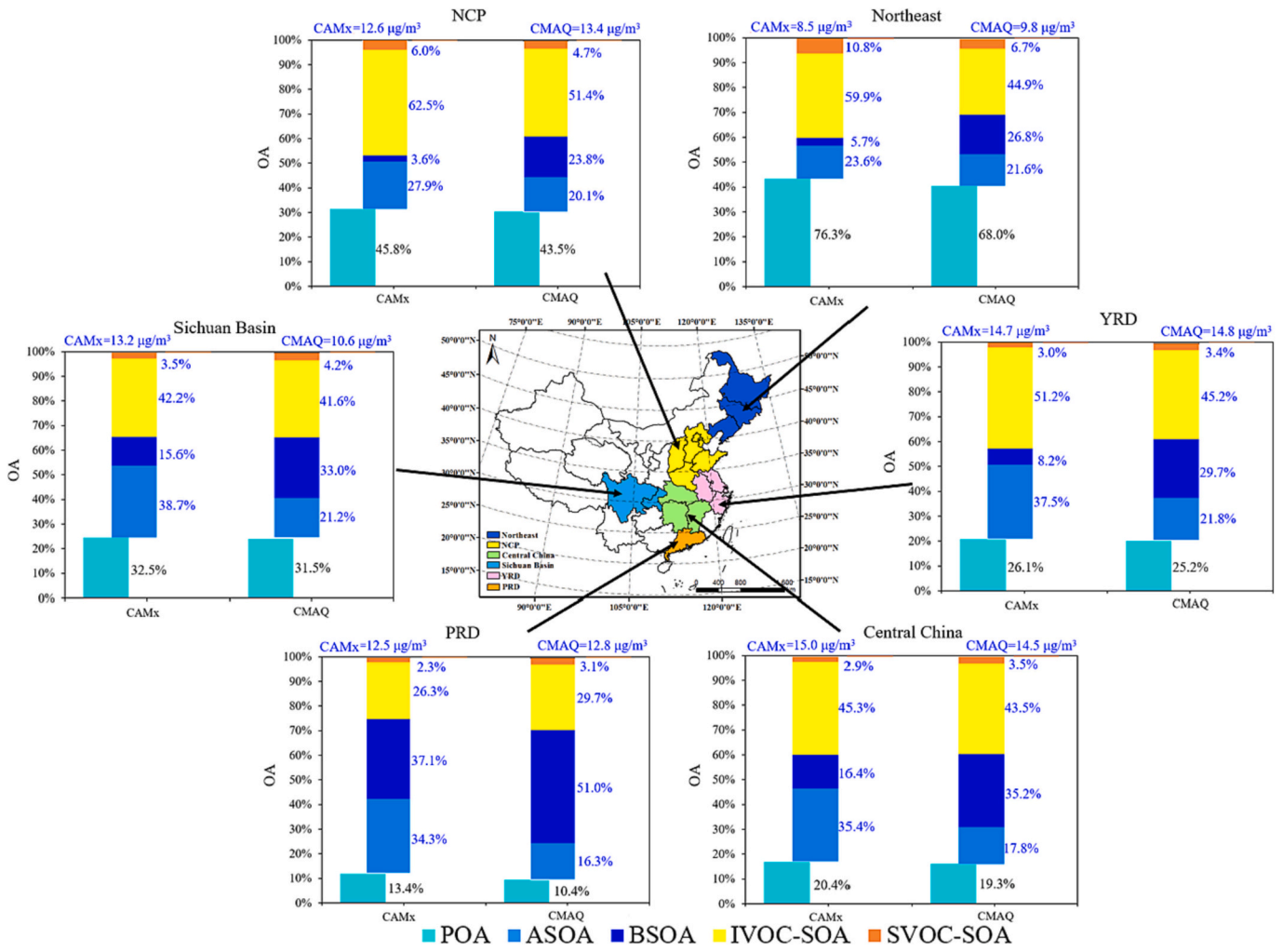

Fig. 5. Domain-averaged OA concentration (labelled on top) and relative contribution of different components (labelled inside Figures) in November 2018 (Note that the relative contribution of ASOA, BSOA, IVOC-SOA, and SVOC-SOA sum to 100 %).

Because of these differences, the relative contribution of ASOA and BSOA varies between the two models. For CAMx simulations, ASOA accounts for 10.9 % (Central China) – 42.1 % (NCP) of total SOA concentration in July and 23.6 % (Northeast China) – 38.7 % (Sichuan Basin) in November. For CMAQ simulation, the relative SOA contribution of ASOA ranges from 4.3 % (Central China) – 15.0 % (NCP) in July and 16.3 % (PRD) – 21.8 % (YRD) in November. In November, CMAQ results suggest that BSOA concentration is always higher than ASOA, while CAMx emphasizes the importance of ASOA more than BSOA.

The two models simulate similar IVOC-SOA concentrations with a maximum of up to 7.3 μg/m^3 in July and 8.7 μg/m^3 in November. The relative contribution of IVOC emissions to SOA ranged from 13.4 % – 13.8 % in PRD to 35.0 % – 42.5 % in NCP for July and 26.3 % – 29.7 % in PRD to 51.4 % – 62.5 % in NCP for November, suggesting an important contribution of IVOC emissions to SOA, especially during November. This finding is consistent with many previous studies that reported the importance of IVOC contribution to SOA (Chang et al., 2022). Compared to other components, both models suggest that SOA generated from SVOC emissions (i.e., SVOC-SOA) are negligible (<0.5 μg/m^3), accounting for <5 % of SOA concentration for most regions. This is different from Miao et al.'s (2021) results which showed much higher SVOC-SOA than IVOC-SOA in eastern China (by as much as two times). However, it should be noted that there still exist large uncertainties in estimating the S/IVOC emissions (Table S2). For example, Liu et al. (2017) obtained a national total of 200.4 Gg IVOC from mobile sources for the year 2015 based on the emission factor method, which is slightly lower than the value (241.2 Gg) reported by Wang et al. (2022) and much higher than Wu's result (134.4 Gg; Wu et al., 2019) based on the IVOC/POA ratio. Using three different estimation methods, Miao et al. (2021) reported a range of 3.8–6.6 Tg anthropogenic IVOC emissions for 2014 in China, which is 30 % – 60 % lower than the value (9.6 Tg) reported by Wu et al. (2021a) for 2016. Regionally, Huang et al. (2021a) calculated the IVOC emissions in the YRD region, and IVOC emissions could be different by a factor of 6.4–69.5 when different methods were applied. The relative contributions from different sources also differ among studies, further increasing the uncertainties of SOA source tracking. Chang et al. (2022) indicate that domestic combustion (including fossil fuel and biomass) and open biomass burning represents the dominant contributors to S/IVOC emissions. In contrast, industry and residential sources contribute 78 % of total S/IVOC emissions, according to Wu et al. (2021b). These results indicate significant uncertainties associated with S/IVOC emission inventory and the subsequent SOA simulation, which warrant more measurement data to better constrain the emission estimation in the future. In this study, we utilized the emission inventory developed by Wu et al. (2021a, 2021b) and focused on the similarities and differences between the models while temporarily ignoring the uncertainties associated with the S/IVOC emission inventory.

3.3. *The impact of SOA aging*

Although a VBS scheme is implemented in both CAMx and CMAQ

models, substantial differences were found in the simulated ASOA concentrations, as shown above, with CAMx predicting much higher values than CMAQ (Fig. 4 and Fig. 5). For example, simulated domain-averaged ASOA concentration in July by CAMx is 5.7 μg/m^3 and 2.9 μg/m^3 over NCP and YRD, respectively, but the corresponding values simulated by CMAQ are only 1.4 μg/m^3 and 0.8 μg/m^3, which are approximately four times lower. The relatively high contribution of ASOA in CAMx (35.6 % ~ 59.1 % of total SOA) is consistent with the study by Li et al. (2022), who reported 48.3 % of SOA was formed from AVOC emissions. Meanwhile, the much lower ASOA concentrations simulated by CMAQ in July over the YRD region (domain-average: 0.8 μg/m^3) are consistent with another CMAQ study conducted by An et al. (2022), who showed minimal SOA contribution (<0.5 μg/m^3) from AVOC for all four seasons. The significant differences in simulated ASOA concentrations between the two models are mainly driven by the different treatments of SOA aging. In the CAMx 1.5D VBS, gas-phase oxidation products in different volatility bins are continuously oxidized by reactions with OH (with an OH rate constant of 2×10^{-11} cm^3/molecule/s) that move mass from higher volatility bins to the next lower volatility bin in a step-wise manner (for example, from C* = 1000 μg/m^3 to C* = 100 μg/m^3 and from C* = 100 μg/m^3 to C* = 10 μg/m^3). The CAMx aging scheme will tend to produce more extensive aging in summer than winter due to higher OH concentrations and greater evaporation of SOA to the gas phase in warmer conditions. In contrast, the VBS in CMAQ AERO7 has no gas-phase oxidation of VBS products and instead converts SOA in VBS bins with C* = 1 μg/m^3 to C* = 100 μg/m^3 directly to non-volatile SOA at a constant rate of 3.4 % per hour. The CMAQ aging scheme, representing oligomerization, will tend to produce more extensive aging in winter than in summer due to greater condensation of SOA in colder conditions. In this study, we can characterize how these schemes differ, but we are unable to assess how well either scheme agrees with the atmosphere because only limited ambient data are available to us for model evaluation.

We investigated how the different treatments of SOA aging in the CMAQ and CAMx VBS schemes influence simulated SOA concentrations by performing simple conceptual calculations outside the models. By doing this, the SOA yields are computed solely based on Pankow's partitioning theory, the total OA concentration, and temperature. Other physical processes (e.g., removal by deposition, atmospheric dispersion) or chemical reactions (i.e., complex radical chemistry) are not included. Based on Pankow's partitioning theory (Pankow, 1994), the SOA yield α from a specific precursor (e.g., benzene) is calculated using Eq. (1):

$$\alpha = \sum_{i}^{N} \beta_i \left(1 + \frac{C_i^*}{C_{OA}}\right)^{-1} \quad (1)$$

where β_i is the mass yields from each volatility bin (i), which are the values listed in Table S12; C_i* is the volatility defined for each bin, and C_{OA} is the total ambient OA concentration; N is the number of volatility bins, and here it equals to 5. We performed separate calculations under both high- and low-NO*x* conditions, where "high-NO*x*" refers to conditions where RO_2 radicals react primarily with NO, whereas under "low-NO*x*" conditions, they react primarily with HO_2 radicals (Seinfeld et al., 1998). We first consider a scenario with no aging in CAMx (CAMx_no-aging). Taking benzene as an example and assuming C_{OA} = 1 μg/m^3 in Eq. (1), SOA mass yield (dimensionless units) from benzene under high and low-NO*x* conditions is 0.009 and 0.029, respectively. With ambient C_{OA} increased by ten times (i.e., C_{OA} = 10 μg/m^3), the gas-particle partition equilibrium shifts more towards the particle phase, and the SOA mass yield for benzene increases to 0.056 and 0.105 for high and low-NO*x*, respectively. Thus we obtain the SOA mass yields for benzene as a function of C_{OA} shown by solid lines in Fig. 6 (similar calculations for toluene and xylene are presented in Fig. S6). Similarly, for CMAQ with no aging (CMAQ_no-aging) and C_{OA} = 1 μg/m^3, the SOA mass yield from benzene is 0.021 and 0.145 under high-and low-NO*x* conditions, respectively. As C_{OA} increased to 10 μg/m^3, SOA mass yield remained unchanged under low-NO*x* conditions and increased by a factor of 3.2 under high-NO*x* conditions, as shown by dashed lines in Fig. 6. When oligomerization (aging) over 6 h is considered in CMAQ (CMAQ_aging), SOA yield for benzene is enhanced by approximately a factor of 2 under the high-NO*x* condition, but there is no enhancement under low-NO*x* condition because the VBS in CMAQ AERO7 always treats this aerosol as being non-volatile and therefore unaffected by aging.

The effect of aging can be much stronger in CAMx than in CMAQ, depending upon the modeled OH radical concentration. We performed a simple offline sensitivity analysis assuming a representative winter OH concentration of 5×10^5 molecules/cm^3. As shown in Fig. 7, an initial VBS distribution favoring higher volatility bins (i.e., towards bin 5) evolves over time with aging (i.e., OH-reaction of the gas-phase fraction in each bin) to favor lower volatility bins (i.e., towards bin 1) which reduces overall volatility and increases aerosol yield. An OH exposure of 10^{10} molecules/cm^3, equal to an exposure time of 5.75 h, was used so that the aging effects shown for CAMx and CMAQ are for a similar duration. With this amount of aging/oxidation effect, the VBS bin molar yields for benzene under high-NO*x* become 0.081, 0.420, 0.324, 0.145, and 0.041 as compared to 0, 0.001, 0.079, 0.148, and 0.222 with no aging (Table S12). These aged yields are converted to SOA mass yields under different total OA concentrations using Eq. (1), as shown by the red symbol line in Fig. 7. For a C_{OA} = 1 μg/m^3 with ~6 h of aging, CAMx simulated a SOA mass yield of 0.322 from benzene under the high-NO*x* condition as opposed to 0.009 without aging, an enhancement greater than a factor of 30. This aging effect becomes even stronger as the

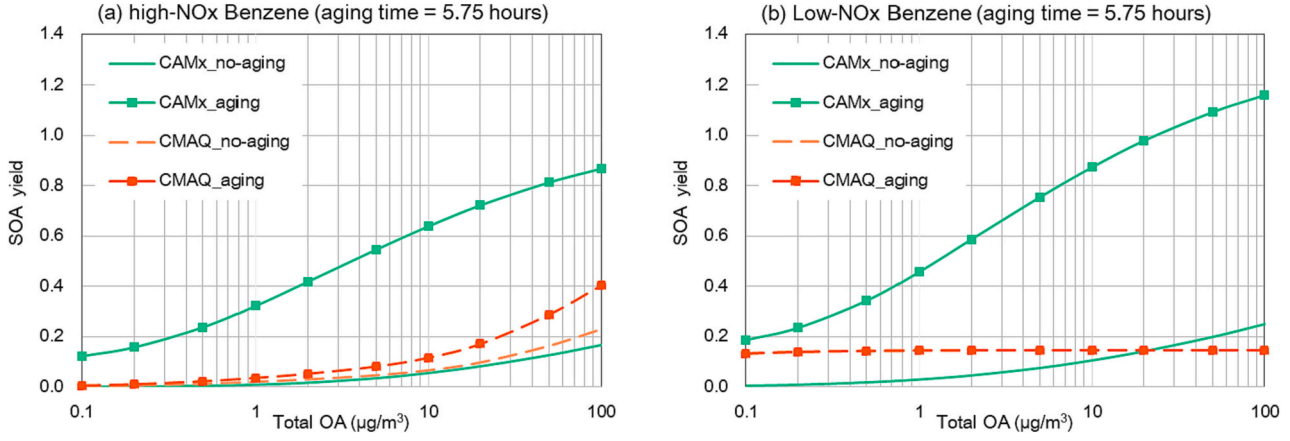

Fig. 6. Conceptual SOA mass yield (μg/m^3 SOA formed per μg/m^3 precursor reacted) from benzene under (a) high- and (b) low-NO*x* conditions by different model configurations. Aging time of 5.75 h is applied for "CAMx_aging" and "CMAQ_aging".

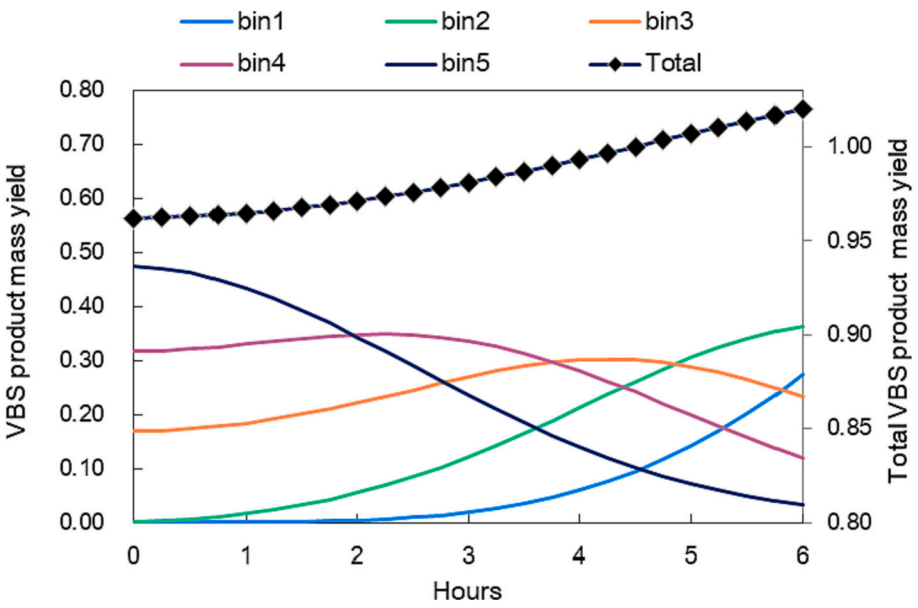

Fig. 7. Aging an initial VBS product distribution that favors higher volatility bins (i.e., near bin 5) using the CAMx 1.5D VBS scheme with [OH] = 5×10^5 molecule/cm^3 and $k_{OH} = 2 \times 10^{-11}$ cm^3/molecule/s changes the volatility distribution to favor lower volatility bins (i.e., near bin 1) and increases total VBS product mass yield (due to oxidation) and would increase aerosol yield (not shown because depends on total OA as illustrated by Fig. 6).

ambient OA concentration increases. These conceptual calculations reveal significant differences in the magnitude of SOA enhancement produced by SOA aging applied within CAMx and CMAQ. However, caution should be taken when interpreting the results calculated by the conceptual model. The aging effect calculated by the offline conceptual model is just an illustration of the aging differences between CAMx and CMAQ, without considering other processes, such as deposition of evaporated SOA (which corresponds to wall-losses in chamber experiments) or atmospheric dilution. Thus the factor of 30 referenced above is a theoretical number that is not directly comparable to chamber experiments. To demonstrate the effect of SOA aging in CAMx simulation, we conducted another set of CAMx base simulations (i.e., without S/IVOC emissions) with no ASOA aging by setting the rate constant of OH with SOA to zero. The spatial distribution of ASOA with and without aging is displayed in Fig. S7. The aging effect in CAMx 1.5D VBS increased ASOA mass by factors of 6– 14.3 in July and 6.3– 9.3 in November, which is on average 2– 3 times stronger than another study conducted by CMAQ 2D-VBS (Zhao et al., 2016). A detailed comparison is included in Supplemental Text 3.

A literature review reveals that different treatments of SOA aging, or no aging, are widespread in the application of VBS schemes. For example, Hayes et al. (2015) applied box models with multi-generating aging parameterization to simulate SOA in Los Angeles during CalNex 2010, which was shown to over-predict urban SOA at photochemical age larger than one day. With several alternate model configurations, Dzepina et al. (2011) predicted SOA mass in Mexico City during MILAGRO 2006 and found that a scenario with a multi-generational SOA aging scheme and no S/IVOC emissions could successfully predict observed SOA but adding S/IVOC emissions resulted in large over-predictions. Jiang et al. (2012) applied WRF-Chem to simulate SOA in China with no aging scheme and concluded that omitting chemical aging of SOA and POA might be the main reason for their underestimation of SOA by up to 75 %. Han et al. (2016) contrasted simulated SOA results based on the VBS scheme with and without considering aging in RAQMS and found that a VBS scheme with aging under-estimated SOA by only 15 %, whereas VBS without aging under-estimated SOA by 70 %.

The examples of differing OA model assumptions and outcomes found in this brief literature review and our simulation results emphasize that model simulations of OA are very sensitive to whether and how SOA aging is represented. A diverse variety of VBS schemes are being used in air quality models, and the predicted OA concentrations may depend upon scheme structure and/or parameters in ways that are difficult to anticipate. Comparing SOA yield curves under idealized conditions (e.g., Fig. 6) can be helpful for comparing different schemes. The range of outcomes produced by current OA schemes illustrates that large uncertainties remain, as well as uncertainties in emission inventories, which should be considered when interpreting results from OA modeling studies. There is a continuing need for sophisticated measurement data to provide better constraints.

4. Conclusions

We applied two commonly used air quality models to simulate SOA concentration and contributions from VOC, IVOC, and SVOC emissions over China for July and November 2018, with emphasis on comparing the models and their sensitivity to assumptions within the VBS schemes. Five OA components were resolved, including POA, SOA formed from biogenic VOC (BSOA), anthropogenic VOC (ASOA), IVOC-SOA, and SVOC-SOA. The POA contribution to total OA is <10 % in July and ranges from 10 % – 40 % in November (except for Northeast China), indicating the dominant role of SOA. Both models suggest that SOA contributions from SVOC emissions are negligible, but IVOC represents an important SOA precursor, especially during November when IVOC becomes the leading SOA contributor for all selected regions except PRD (accounting for 26 % to 30 % in PRD and 45 % to 63 % in NCP). Although our modeling results are subject to the uncertainties associated with the S/IVOC emission inventory, as discussed above, the consistently large contribution of IVOC emissions to total OA indicates that future control policies should aim at reducing IVOC emissions as well as traditional VOC emissions. More measurement data to better constrain the emission estimation are warranted in the future.

While both models show generally consistent results in terms of the spatial distributions and seasonal variations of the resolved OA components, differences were found with simulated ASOA and BSOA concentrations. CMAQ tends to estimate higher BSOA concentration, while CAMx generates more ASOA. As a result, CMAQ results suggest that BSOA concentration is always higher than ASOA in November, while CAMx emphasizes the importance of ASOA. With the help of a

conceptual model, we demonstrate that the higher ASOA simulated by CAMx is attributable to the aging effect on ASOA implemented in CAMx. In the CAMx 1.5D VBS, SOA formed in higher volatility bins is assumed to undergo further gas-phase oxidation by OH into lower volatility bins. It is estimated that with 6 h of aging at a representative wintertime OH concentration of 5×10^5 molecules/cm^3, SOA aging could enhance ASOA concentration by an order of magnitude, or more, depending on the total ambient OA concentration. The VBS in CMAQ AERO7 implements a different SOA aging scheme that represents particle-phase oligomerization and has smaller impacts on total OA, or no impact, than the CAMx 1.5D VBS aging scheme. A brief literature survey reveals that a diverse variety of VBS schemes (aging or no-aging) and/or parameters are being used in air quality models and could greatly affect model simulations of OA in ways that may be difficult to anticipate.

Several limitations in the current study warrant follow-up work. First, only observed OC/EC data at a few available were used for model validation. Future studies should apply more advanced monitoring data that resolve OA constituents to improve model evaluation and development when these data become available. Second, the emission inventory utilized in this study was not comprehensive. For instance, the volatile chemical products (VCP), recently reported as an increasingly important SOA contributor, were not included. Lastly, the current work only contrasts two commonly used air quality models. A comprehensive inter-model comparison incorporating more models would benefit the modeling community.

Financial support

This study has been supported by the National Natural Science Foundation of China (Grant NOs. 42005112, 42075144, 41105102, 41875161) and the Shanghai Sail Program (no. 19YF1415600).

CRediT authorship contribution statement

Ling Huang: Conceptualization, Methodology, Software, Visualization, Validation, Writing-original draft preparation,

Hanqing Liu: Methodology, Software, Visualization, Validation, Data curation, Writing-original draft preparation.

Greg Yarwood: Software, Methodology, Writing-reviewing and editing.

Gary Wilson: Software, Methodology.

Jun Tao, Zhiwei Han, Dongsheng Ji: Data curation.

Yangjun Wang: Writing-reviewing and editing.

Li Li: Conceptualization, Funding Acquisition, Writing-reviewing and editing

Declaration of competing interest

The authors declare that they have no known competing financial interests or personal relationships that could have appeared to influence the work reported in this paper.

Data availability

Data will be made available on request.

Appendix A. Supplementary data

Supplementary data to this article can be found online at https://doi.org/10.1016/j.scitotenv.2023.166162.

References

An, J., Huang, C., Huang, D., Qin, M., Liu, H., Yan, R., Qiao, L., Zhou, M., Li, Y., Zhu, S., Wang, Q., Wang, H., 2022. Sources of organic aerosols in eastern China: a modeling study with high-resolution intermediate-volatility and semivolatile organic compound emissions. Atmos. Chem. Phys. Discuss. 2022, 1–44.

Appel, K.W., Bash, J.O., Fahey, K.M., Foley, K.M., Gilliam, R.C., Hogrefe, C., Hutzell, W. T., Kang, D., Mathur, R., Murphy, B.N., Napelenok, S.L., Nolte, C.G., Pleim, J.E., Pouliot, G.A., Pye, H.O.T., Ran, L., Roselle, S.J., Sarwar, G., Schwede, D.B., Sidi, F.I., Spero, T.L., Wong, D.C., 2021. The community multiscale air quality (CMAQ) model versions 5.3 and 5.3.1: system updates and evaluation. Geosci. Model Dev. 14 (5), 2867–2897.

Cao, J.J., Lee, S.C., Ho, K.F., Zou, S.C., Fung, K., Li, Y., Watson, J.G., Chow, J.C., 2004. Spatial and seasonal variations of atmospheric organic carbon and elemental carbon in Pearl River Delta region, China. Atmos. Environ. 38 (27), 4447–4456.

Cao, J.Y., Qiu, X.H., Peng, L., Gao, J., Wang, F.Y., Yan, X., 2022. Impacts of the differences in PM2.5 air quality improvement on regional transport and health risk in Beijing-Tianjin-Hebei region during 2013-2017. Chemosphere 297.

Carlton, A.G., Turpin, B.J., Altieri, K.E., Seitzinger, S.P., Mathur, R., Roselle, S.J., Weber, R.J., 2008. CMAQ model performance enhanced when in-cloud secondary organic aerosol is included: comparisons of organic carbon predictions with measurements. Environ. Sci. Technol. 42 (23), 8798–8802.

Carlton, A.G., Bhave, P.V., Napelenok, S.L., Edney, E.D., Sarwar, G., Pinder, R.W., Pouliot, G.A., Houyoux, M., 2010. Model representation of secondary organic aerosol in CMAQv4.7. Environ. Sci. Technol. 44 (22), 8553–8560.

Castro, L.M., Pio, C.A., Harrison, R.M., Smith, D.J.T., 1999. Carbonaceous aerosol in urban and rural European atmospheres: estimation of secondary organic carbon concentrations. Atmos. Environ. 33 (17), 2771–2781.

Chang, X., Zhao, B., Zheng, H., Wang, S., Cai, S., Guo, F., Gui, P., Huang, G., Wu, D., Han, L., Xing, J., Man, H., Hu, R., Liang, C., Xu, Q., Qiu, X., Ding, D., Liu, K., Han, R., Robinson, A.L., Donahue, N.M., 2022. Article full-volatility emission framework corrects missing and underestimated secondary organic aerosol sources. One Earth 5 (4), 403–412.

Donahue, N.M., Robinson, A.L., Stanier, C.O., Pandis, S.N., 2006. Coupled partitioning, dilution, and chemical aging of semivolatile organics. Environ. Sci. Technol. 40 (8), 2635–2643.

Dzepina, K., Cappa, C.D., Volkamer, R.M., Madronich, S., DeCarlo, P.F., Zaveri, R.A., Jimenez, J.L., 2011. Modeling the multiday evolution and aging of secondary organic aerosol during MILAGRO 2006. Environ. Sci. Technol. 45 (8), 3496–3503.

Han, Z., Xie, Z., Wang, G., Zhang, R., Tao, J., 2016. Modeling organic aerosols over East China using a volatility basis-set approach with aging mechanism in a regional air quality model. Atmos. Environ. 124, 186–198.

Hayes, P.L., Carlton, A.G., Baker, K.R., Ahmadov, R., Washenfelder, R.A., Alvarez, S., Rappenglueck, B., Gilman, J.B., Kuster, W.C., de Gouw, J.A., Zotter, P., Prevot, A.S. H., Szidat, S., Kleindienst, T.E., Offenberg, J.H., Ma, P.K., Jimenez, J.L., 2015. Modeling the formation and aging of secondary organic aerosols in Los Angeles during CalNex 2010. Atmos. Chem. Phys. 15 (10), 5773–5801.

Hu, J., Wang, P., Ying, Q., Zhang, H., Chen, J., Ge, X., Li, X., Jiang, J., Wang, S., Zhang, J., Zhao, Y., Zhang, Y., 2017. Modeling biogenic and anthropogenic secondary organic aerosol in China. Atmos. Chem. Phys. 17 (1), 77–92.

Huang, L., Wang, Q., Wang, Y., Emery, C., Zhu, A., Zhu, Y., Yin, S., Yarwood, G., Zhang, K., Li, L., 2021a. Simulation of secondary organic aerosol over the Yangtze River Delta region: the impacts from the emissions of intermediate volatility organic compounds and the SOA modeling framework. Atmos. Environ. 246.

Huang, L., Zhu, Y., Wang, Q., Zhu, A., Liu, Z., Wang, Y., Allen, D.T., Li, L., 2021b. Assessment of the effects of straw burning bans in China: emissions, air quality, and health impacts. Sci. Total Environ. 789.

Huang, L., Zhu, Y., Zhai, H., Xue, S., Zhu, T., Shao, Y., Liu, Z., Emery, C., Yarwood, G., Wang, Y., Fu, J., Zhang, K., Li, L., 2021c. Recommendations on benchmarks for numerical air quality model applications in China - part 1: PM2.5 and chemical species. Atmos. Chem. Phys. 21 (4), 2725–2743.

Huang, L., Zhu, Y., Liu, H., Wang, Y., Allen, D.T., Ooi, M.C.G., Manomaiphiboon, K., Latif, M.T., Chan, A., Li, L., 2023. Assessing the contribution of open crop straw burning to ground-level ozone and associated health impacts in China and the effectiveness of straw burning bans. Environ. Int. 171.

Jiang, F., Liu, Q., Huang, X., Wang, T., Zhuang, B., Xie, M., 2012. Regional modeling of secondary organic aerosol over China using WRF/Chem. J. Aerosol Sci. 43 (1), 57–73.

Kampa, M., Castanas, E., 2008. Human health effects of air pollution. Environ. Pollut. 151 (2), 362–367.

Koo, B., Knipping, E., Yarwood, G., 2014. 1.5-dimensional volatility basis set approach for modeling organic aerosol in CAMx and CMAQ. Atmos. Environ. 95, 158–164.

Li, H., Wang, Q.G., Yang, M., Li, F., Wang, J., Sun, Y., Wang, C., Wu, H., Qian, X., 2016a. Chemical characterization and source apportionment of PM2.5 aerosols in a megacity of Southeast China. Atmos. Res. 181, 288–299.

Li, L., An, J.Y., Shi, Y.Y., Zhou, M., Yan, R.S., Huang, C., Wang, H.L., Lou, S.R., Wang, Q., Lu, Q., Wu, J., 2016b. Source apportionment of surface ozone in the Yangtze River Delta, China in the summer of 2013. Atmos. Environ. 144, 194–207.

Li, M., Zhang, Q., Kurokawa, J.-I., Woo, J.-H., He, K., Lu, Z., Ohara, T., Song, Y., Streets, D.G., Carmichael, G.R., Cheng, Y., Hong, C., Huo, H., Jiang, X., Kang, S., Liu, F., Su, H., Zheng, B., 2017a. MIX: a mosaic Asian anthropogenic emission inventory under the international collaboration framework of the MICS-Asia and HTAP. Atmos. Chem. Phys. 17 (2), 935–963.

Li, J., Zhang, M., Wu, F., Sun, Y., Tang, G., 2017b. Assessment of the impacts of aromatic VOC emissions and yields of SOA on SOA concentrations with the air quality model RAMS-CMAQ. Atmos. Environ. 158, 105–115.

Li, J., Han, Z., Wu, J., Tao, J., Li, J., Sun, Y., Liang, L., Liang, M., Wang, Q.G., 2022. Secondary organic aerosol formation and source contributions over East China in summertime. Environ. Pollut. 306.

Lin, J., An, J., Qu, Y., Chen, Y., Li, Y., Tang, Y., Wang, F., Xiang, W., 2016. Local and distant source contributions to secondary organic aerosol in the Beijing urban area in summer. Atmos. Environ. 124, 176–185.

Liu, Y.Z., Jia, R., Dai, T., Xie, Y.K., Shi, G.Y., 2014. A review of aerosol optical properties and radiative effects. J. Meteorol. Res. 28 (6), 1003–1028.
Liu, H., Man, H., Cui, H., Wang, Y., Deng, F., Wang, Y., Yang, X., Xiao, Q., Zhang, Q., Ding, Y., He, K., 2017. An updated emission inventory of vehicular VOCs and IVOCs in China. Atmos. Chem. Phys. 17 (20), 12709–12724.
Miao, R., Chen, Q., Shrivastava, M., Chen, Y., Zhang, L., Hu, J., Zheng, Y., Liao, K., 2021. Process-based and observation-constrained SOA simulations in China: the role of semivolatile and intermediate-volatility organic compounds and OH levels. Atmos. Chem. Phys. 21 (21), 16183–16201.
Murphy, D.M., Cziczo, D.J., Froyd, K.D., Hudson, P.K., Matthew, B.M., Middlebrook, A. M., Peltier, R.E., Sullivan, A., Thomson, D.S., Weber, R.J., 2006. Single-particle mass spectrometry of tropospheric aerosol particles. J. Geophys. Res.-Atmos. 111 (D23).
Murphy, B.N., Woody, M.C., Jimenez, J.L., Carlton, A.M.G., Hayes, P.L., Liu, S., Ng, N.L., Russell, L.M., Setyan, A., Xu, L., Young, J., Zaveri, R.A., Zhang, Q., Pye, H.O.T., 2017. Semivolatile POA and parameterized total combustion SOA in CMAQv5.2: impacts on source strength and partitioning. Atmos. Chem. Phys. 17 (18), 11107–11133.
Nenes, A., Pandis, S.N., Pilinis, C., 1998. ISORROPIA: a new thermodynamic equilibrium model for multiphase multicomponent inorganic aerosols. Aquat. Geochem. 4 (1), 123–152.
Odum, J.R., Hoffmann, T., Bowman, F., Collins, D., Flagan, R.C., Seinfeld, J.H., 1996. Gas/particle partitioning and secondary organic aerosol yields. Environ. Sci. Technol. 30 (8), 2580–2585.
Pande, P., Shrivastava, M., Shilling, J.E., Zelenyuk, A., Zhang, Q., Chen, Q., Ng, N.L., Zhang, Y., Takeuchi, M., Nah, T., Rasool, Q.Z., Zhang, Y., Zhao, B., Liu, Y., 2022. Novel application of machine learning techniques for rapid SourceApportionment of aerosol mass spectrometer datasets. ACS Earth Space Chem. 6 (4), 932–942.
Pankow, J.F., 1994. An absorption model of the gas/aerosol partitioning involved in the formation of secondary organic aerosol. Atmos. Environ. 28 (2), 189–193.
Pye, H.O.T., Pouliot, G.A., 2012. Modeling the role of alkanes, polycyclic aromatic hydrocarbons, and their oligomers in secondary organic aerosol formation. Environ. Sci. Technol. 46 (11), 6041–6047.
Pye, H.O.T., Chan, A.W.H., Barkley, M.P., Seinfeld, J.H., 2010. Global modeling of organic aerosol: the importance of reactive nitrogen (NOx and NO3). Atmos. Chem. Phys. 10 (22), 11261–11276.
Pye, H.O.T., Pinder, R.W., Piletic, I.R., Xie, Y., Capps, S.L., Lin, Y.-H., Surratt, J.D., Zhang, Z., Gold, A., Luecken, D.J., Hutzell, W.T., Jaoui, M., Offenberg, J.H., Kleindienst, T.E., Lewandowski, M., Edney, E.O., 2013. Epoxide pathways improve model predictions of isoprene markers and reveal key role of acidity in aerosol formation. Environ. Sci. Technol. 47 (19), 11056–11064.
Pye, H.O.T., Luecken, D.J., Xu, L., Boyd, C.M., Ng, N.L., Baker, K.R., Ayres, B.R., Bash, J. O., Baumann, K., Carter, W.P.L., Edgerton, E., Fry, J.L., Hutzell, W.T., Schwede, D.B., Shepson, P.B., 2015. Modeling the current and future roles of particulate organic nitrates in the southeastern United States. Environ. Sci. Technol. 49 (24), 14195–14203.
Pye, H.O.T., Murphy, B.N., Xu, L., Ng, N.L., Carlton, A.G., Guo, H., Weber, R., Vasilakos, P., Appel, K.W., Budisulistiorini, S.H., Surratt, J.D., Nenes, A., Hu, W., Jimenez, J.L., Isaacman-VanWertz, G., Misztal, P.K., Goldstein, A.H., 2017. On the implications of aerosol liquid water and phase separation for organic aerosol mass. Atmos. Chem. Phys. 17 (1), 343–369.
Pye, H.O.T., Ward-Caviness, C.K., Murphy, B.N., Appel, K.W., Seltzer, K.M., 2021. Secondary organic aerosol association with cardiorespiratory disease mortality in the United States. Nat. Commun. 12 (1).
Qin, Y., Ye, J., Ohno, P., Liu, P., Wang, J., Fu, P., Zhou, L., Li, Y.J., Martin, S.T., Chan, C. K., 2022. Assessing the nonlinear effect of atmospheric variables on primary and oxygenated organic aerosol concentration using machine learning. ACS Earth Space Chem. 6 (4), 1059–1066.
Ramboll, 2021. User's Guide: Comprehensive Air quality Model with extensions, Version 7.1. Available at: www.camx.com. Accessed on 25th September 2021.
Schreck, J.S., Becker, C., Gagne, D.J., Lawrence, K., Wang, S., Mouchel-Vallon, C., Choi, J., Hodzic, A., 2022. Neural network emulation of the formation of organic aerosols based on the explicit GECKO-A chemistry model. J. Adv. Modeling Earth Syst. 14 (10).
Seinfeld, J.H., Pandis, S.N., Noone, K.J.J.P.T., 1998. Atmospheric chemistry and physics: from air pollution to. Climate Change 51, 88–90.
Shi, G., Peng, X., Liu, J., Tian, Y., Song, D., Yu, H., Feng, Y., Russell, A.G., 2016. Quantification of long-term primary and secondary source contributions to carbonaceous aerosols. Environ. Pollut. 219, 897–905.
Skamarock, W.C., Klemp, J.B., 2008. A time-split nonhydrostatic atmospheric model for weather research and forecasting applications. J. Comput. Phys. 227 (7), 3465–3485.
U.S. EPA: (2020) United States environmental protection agency. (2020). CMAQ (version 5.3.2) [software]. Available from doi:https://doi.org/10.5281/zenodo.4081737.
Wang, F., Zhang, Z., Wang, G., Wang, Z., Li, M., Liang, W., Gao, J., Wang, W., Chen, D., Feng, Y., Shi, G., 2022. Machine learning and theoretical analysis release the non-linear relationship among ozone, secondary organic aerosol and volatile organic compounds. J. Environ. Sci. 114, 75–84.
Wu, L., Ling, Z., Liu, H., Shao, M., Lu, S., Wu, L., Wang, X., 2021a. A gridded emission inventory of semivolatile and intermediate volatility organic compounds in China. Sci. Total Environ. 761.
Wu, L., Ling, Z., Shao, M., Liu, H., Lu, S., Zhou, S., Guo, J., Mao, J., Hang, J., Wang, X., 2021b. Roles of Semivolatile/intermediate-volatility organic compounds on SOA formation over China during a pollution episode: sensitivity analysis and implications for future studies. J. Geophys. Res.-Atmos. 126 (8).
Wu, L., Wang, X., Lu, S., Shao, M., Ling, Z., 2019. Emission inventory of semi-volatile and intermediate-volatility organic compounds and their effects on secondary organic aerosol over the Pearl River Delta region. Atmospheric Chemistry and Physics 19 (12), 8141–8161.
Xie, Y.-B., Chen, J., Li, W., 2014. An assessment of PM2.5 related health risks and impaired values of Beijing residents in a consecutive high-level exposure during heavy haze days. Huan jing ke xue= Huanjing kexue 35 (1), 1–8.
Xu, L., Pye, H.O.T., He, J., Chen, Y., Murphy, B.N., Ng, N.L., 2018. Experimental and model estimates of the contributions from biogenic monoterpenes and sesquiterpenes to secondary organic aerosol in the southeastern United States. Atmos. Chem. Phys. 18 (17), 12613–12637.
Yan, Y.Y., Zhou, Y., Kong, S.F., Lin, J.T., Wu, J., Zheng, H., Zhang, Z.X., Song, A.L., Bai, Y.Q., Ling, Z., Liu, D.T., Zhao, T.L., 2021. Effectiveness of emission control in reducing PM2.5 pollution in central China during winter haze episodes under various potential synoptic controls. Atmos. Chem. Phys. 21 (4), 3143–3162.
Yao, T., Li, Y., Gao, J., Fung, J.C.H., Wang, S., Li, Y., Chan, C.K., Lau, A.K.H., 2020. Source apportionment of secondary organic aerosols in the Pearl River Delta region: contribution from the oxidation of semivolatile and intermediate volatility primary organic aerosols. Atmos. Environ. 222.
Yarwood, G., Jung, J., Whitten, G.Z., Heo, G., Mellberg, J., Estes, M., 2010. Updates to the Carbon Bond Mechanism for Version, 6 (CB6).
Zhang, L., Brook, J.R., Vet, R., 2003. A revised parameterization for gaseous dry deposition in air-quality models. Atmos. Chem. Phys. 3, 2067–2082.
Zhang, Q., Jimenez, J.L., Canagaratna, M.R., Allan, J.D., Coe, H., Ulbrich, I., Alfarra, M. R., Takami, A., Middlebrook, A.M., Sun, Y.L., Dzepina, K., Dunlea, E., Docherty, K., DeCarlo, P.F., Salcedo, D., Onasch, T., Jayne, J.T., Miyoshi, T., Shimono, A., Hatakeyama, S., Takegawa, N., Kondo, Y., Schneider, J., Drewnick, F., Borrmann, S., Weimer, S., Demerjian, K., Williams, P., Bower, K., Bahreini, R., Cottrell, L., Griffin, R.J., Rautiainen, J., Sun, J.Y., Zhang, Y.M., Worsnop, D.R., 2007. Ubiquity and dominance of oxygenated species in organic aerosols in anthropogenically-influenced northern hemisphere midlatitudes. Geophys. Res. Lett. 34 (13).
Zhang, Y., Li, X., Nie, T., Qi, J., Chen, J., Wu, Q., 2018. Source apportionment of PM2.5 pollution in the central six districts of Beijing, China. J. Clean. Prod. 174, 661–669.
Zhang, Q., Zheng, Y., Tong, D., Shao, M., Wang, S., Zhang, Y., Xu, X., Wang, J., He, H., Liu, W., Ding, Y., Lei, Y., Li, J., Wang, Z., Zhang, X., Wang, Y., Cheng, J., Liu, Y., Shi, Q., Yan, L., Geng, G., Hong, C., Li, M., Liu, F., Zheng, B., Cao, J., Ding, A., Gao, J., Fu, Q., Huo, J., Liu, B., Liu, Z., Yang, F., He, K., Hao, J., 2019. Drivers of improved PM2.5 air quality in China from 2013 to 2017. Proc. Natl. Acad. Sci. U. S. A. 116 (49), 24463–24469.
Zhao, B., Wang, S., Donahue, N.M., Jathar, S.H., Huang, X., Wu, W., Robinson, A.L., 2016. Quantifying the effect of organic aerosol aging and intermediate-volatility emissions on regional-scale aerosol pollution in China. Sci. Rep. 6 (1), 28815.
Zheng, B., Tong, D., Li, M., Liu, F., Hong, C., Geng, G., Li, H., Li, X., Peng, L., Qi, J., Yan, L., Zhang, Y., Zhao, H., Zheng, Y., He, K., Zhang, Q., 2018. Trends in China's anthropogenic emissions since 2010 as the consequence of clean air actions. Atmos. Chem. Phys. 18 (19), 14095–14111.